Single-chain and condensed-state behavior of hnRNPA1 from molecular simulations

D. Janka Bauer,[†] Lukas S. Stelzl,[‡,†,¶] and Arash Nikoubashman[*,†]

[†]*Institute of Physics, Johannes Gutenberg University Mainz, Staudingerweg 7, 55128 Mainz, Germany*

[‡]*Faculty of Biology, Johannes Gutenberg University Mainz, 55128 Mainz, Germany*

[¶]*Institute of Molecular Biology (IMB), 55128 Mainz, Germany*

E-mail: anikouba@uni-mainz.de

Abstract

Intrinsically disordered proteins (IDPs) are essential components for the formation of membraneless organelles, which play key functional and regulatory roles within biological systems. These complex assemblies form and dissolve spontaneously over time *via* liquid-liquid phase separation of IDPs. Mutations in their amino acid sequence can alter their phase behavior, which has been linked to the emergence of severe diseases such as cancer and neurodegenerative diseases including amyotrophic lateral sclerosis. In this work, we study the conformation and phase behavior of a low-complexity domain of heterogeneous nuclear ribonucleoprotein A1 (hnRNPA1), using coarse-grained implicit solvent molecular dynamics simulations. We systematically analyze how these properties are affected by the number of aromatic residues within the examined sequences. We find a significant compaction of the chains and an increase in the critical temperature with increasing number of aromatic residues within the IDPs. Both observations strongly support the hypothesis that aromatic residues play a dominant role for

condensation, which is further corroborated by a detailed analysis of the intermolecular contacts. Interestingly, we observe density inhomogeneities within the condensates near criticality, which are driven by electrostatic interactions. Comparing single-chain and condensed state simulations, we find distinct differences in the conformations of individual chains. By establishing quantitative comparisons to the experimental phase behavior, we start to critically assess the reliability of coarse-grained IDP models.

Keywords

phase behavior, conformation, disordered protein chains, molecular simulations

1 Introduction

The discovery that liquid-liquid phase separation gives rises to biomolecular condensates and membraneless organelles is revolutionizing our understanding of cell biology [1,2] and provides new perspectives for studying self-assembly on the nanoscale. [3] Frequently, this phase separation is driven by disordered regions of biomacromolecules or intrinsically disordered proteins (IDPs). These biomolecular condensates can be liquid and highly dynamic, but can also maturate and solidify. [2,4] Dysregulation of liquid-liquid phase separation and formation of toxic aggregates play important roles in neurodegenerative diseases and ageing. [5–7] In addition, the equilibrium between dilute and condensed phases may have important implications on protein function in health and disease as these two different states of matter can potentially underpin quite different biological functions. [8] It is of particular interest to elucidate the single-chain behavior in dilute solutions and in condensates, as such knowledge could be useful for predicting, *e.g.*, the conformation and phase behavior of IDPs based on their specific sequence. In the past few years, important progress has been made in this regard, but there are still many open questions and seemingly conflicting results: [9] For example, high-resolution nuclear magnetic resonance experiments on dense IDP phases have

revealed that local structures on the scale of individual residues can be highly similar in dilute solution and condensates,[10–12] whereas recent electron paramagnetic resonance[13] and single-molecule Förster resonance energy transfer[14] experiments have observed changes in the global structures and overall extension of IDPs in dense phases compared to dilute phases.

Computer simulations are valuable tools for studying the conformation of IDPs in solution and in condensates, as they provide molecular-level insights. Further, simulations are highly suited for characterizing phase-separated biomolecular condensates, their material properties, the underlying molecular interactions and the implications of the formation of phase-separated condensates for cell biology.[7,15–20] Atomistic simulations provide crucial information on residual structures of dilute IDPs and how chemical details modulate local and global conformations, which can be important for understanding biological function.[21–25] However, despite encouraging progress over the past few years,[7,16,26] such atomistically detailed simulations are still prohibitively time-consuming for studying phase separation and phase-separated condensates. Coarse-grained protein models can greatly speed up simulations, allowing for larger system sizes and longer simulation times. Further, such simplified models can help to reveal the essential elements that shape molecular systems.[17,27] The development of such coarse-grained models is a highly active field, and great strides have been made to establish transferable force-fields which can capture the sequence specific conformation and phase behavior of IDPs.[15,20,28–33] In sticker and spacer models, some amino acid residues—the stickers—engage in contacts stabilizing condensates, whereas the remaining residues serve as inert spacers.[3,34–36] These conceptually simple models are motivated by the experimental observation that favorable (noncovalent) inter-chain contacts are predominantly driven by only few residue types.[37] Within this framework, the material properties of biomolecular condensates are primarily dictated by the valence and distribution of stickers, and valuable insights have been gained through it for rationalizing many important experimental trends.

The low-complexity domain of heterogeneous nuclear ribonucleoprotein A1 (hnRNPA1)

(A1-LCD) is a well characterized model system which provides an ideal test ground to benchmark and validate computational approaches, and to elucidate how sequence characteristics determine dilute and dense phase behavior.[20,38] Recently, Martin *et al.* investigated the single-chain conformation and phase behavior of A1-LCD through both experiments and simulations.[39] They studied the wild-type as well as several variants, finding more compact polymer conformations for sequences containing more aromatic residues. Further, the critical temperature of the solutions increased significantly with increasing number of aromatic residues. These observations were rationalized *via* Monte Carlo simulations of a sticker-spacer lattice model, in which the aromatic Phenylalanine (F) and Tyrosine (Y) residues were assigned as stickers. To better understand the role of aromatic residues for the phase behavior of protein chains, we performed molecular simulations using a protein-agnostic coarse-grained IDP model,[15] and compared the resulting phase behavior directly to experimental data. The residue-level coarse-grained model which we employed may help to better understand the context-dependent interactions of amino acids such as Arginine (R), which is known to be a sequence-specfic sticker.[40] The net positive charge of A1-LCD chains also motivated us to understand the effect of charge-charge interactions in A1-LCD condensates, which is possible in the employed framework of the coarse-grained model of Dignon *et al.*[15] Furthermore, we characterized the chain conformations in both the dilute and dense phases and identified the relevant contacts driving phase separation.

2 Model and Methods

We model the A1-LCD protein chains using the coarse-grained hydrophobicity scale (HPS) model developed by Dignon *et al.*,[15] where each amino acid is represented as one spherical bead of diameter σ_i and mass m_i. At this level of coarse-graining, each A1-LCD chain consists of $N = 137$ particles. The solvent is modeled implicitly, and the hydrophobicity of

the various residues is included in the effective monomer-monomer pair interaction

$$U_{\mathrm{mm}}(\lambda_{ij}, r) = \begin{cases} U_{\mathrm{LJ}} + (1-\lambda_{ij})\varepsilon & r \leq 2^{1/6}\sigma_{ij} \\ \lambda_{ij} U_{\mathrm{LJ}} & \text{else,} \end{cases} \tag{1}$$

where U_{LJ} is the standard Lennard-Jones (LJ) potential

$$U_{\mathrm{LJ}}(r) = \begin{cases} 4\varepsilon\left[(\sigma_{ij}/r)^{12} - (\sigma_{ij}/r)^{6}\right] & r \leq r_{\mathrm{c}}^{\mathrm{LJ}} \\ 0 & \text{else,} \end{cases} \tag{2}$$

with interaction strength $\varepsilon = 0.2\,\mathrm{kcal/mol}$ and cutoff radius $r_{\mathrm{c}}^{\mathrm{LJ}} = 2.0\,\mathrm{nm}$.[15] The dimensionless parameter $0 \leq \lambda_{ij} \leq 1$ controls the attraction between a pair of beads of type i and j, and thus their effective hydrophobicity. Choosing $\lambda_{ij} = 0$ for all pairs renders U_{mm} purely repulsive, resulting in good solvent conditions for the polymer. (Note that bonded monomers were excluded from the pair interactions.) Arithmetic averages are used as the mixing rule for the bead diameters and hydrophobicity scale, *i.e.*, $\sigma_{ij} = (\sigma_i + \sigma_j)/2$ and $\lambda_{ij} = (\lambda_i + \lambda_j)/2$, respectively. The bead diameters σ_i have been set according to the van der Waals volume of the corresponding amino acids, while the λ_i are based on the hydrophobicity scale developed by Kapcha and Rossky.[41]

The employed HPS model also includes a simplified treatment of (screened) electrostatics through the pair potential

$$U_{\mathrm{el}}(r) = \frac{q_i q_j}{4\pi\epsilon_0\epsilon_{\mathrm{r}} r} \exp\left(-r/\lambda_{\mathrm{D}}\right), \tag{3}$$

with charges q_i and q_j, Debye screening length λ_{D}, vacuum permittivity ϵ_0, and relative dielectric constant ϵ_{r}. To reproduce close to physiological conditions (100 mmol/L salt concentration in water), we chose $\lambda_{\mathrm{D}} = 1\,\mathrm{nm}$ and $\epsilon_{\mathrm{r}} = 80$. Further, the potential U_{el} has been truncated at $r_{\mathrm{c}}^{\mathrm{el}} = 3.5\,\mathrm{nm}$.

Bonded interactions are modeled using a harmonic potential

$$U_{\mathrm{b}}(r) = \frac{k}{2}\left(r - r_0\right)^2 \tag{4}$$

with spring constant $k = 2000\,\mathrm{kcal/(mol\,nm^2)}$ and equilibrium bond length $r_0 = 0.38\,\mathrm{nm}$.

Molecular dynamics (MD) simulations were performed in the canonical ensemble, where the temperature T was controlled *via* a Langevin thermostat. The equations of motion were integrated using a velocity Verlet scheme with time step $\Delta t = 10\,\mathrm{fs}$. All simulations were conducted on graphics processing units using the HOOMD-blue software package[42] (v. 2.9.6) extended with azplugins (v. 0.10.2).[43] All snapshots rendered using Visual Molecular Dynamics (version 1.9.3).[44]

3 Results

In this work, we focus on the wild-type (WT) of A1-LCD and three of its variants with fewer ($\mathrm{Aro^-}$ and $\mathrm{Aro^{--}}$) and more ($\mathrm{Aro^+}$) aromatic residues (the employed amino acid sequences are identical to the ones from Ref. 39 and are included in the Supporting Information). To establish reference points, we also performed simulations of ideal chains (achieved by disabling all non-bonded interactions) and protein chains in a good solvent (achieved by setting $q_i = 0$ and $\lambda_i = 0$ for all monomers i). These reference chains have the same contour length as the A1-LCD protein chains. We also ran an additional set of simulations of the A1-LCD (WT) sequence at infinite dilution with the re-parameterized HPS model of Tesei *et al.* (see Sec. 3.1).[20]

The conformation and structure formation of amphiphilic heteropolymers, such as protein chains, depend not only on the fraction of hydrophobic residues, f, but also on their location in the sequence.[45–47] For example, diblock amphiphiles with $f = 0.6$ self-assemble into spherical micelles, whereas chains with uniformly distributed hydrophobic monomers merge into liquid droplets at the same f.[45] To characterize the fraction and distribution of

hydrophobic residues in the investigated protein chains, we calculated the sequence hydropathy decoration (SHD) parameter for each variant[46]

$$\lambda_{\mathrm{SHD}} = \frac{1}{N}\sum_{i}\sum_{j>i}(\lambda_i + \lambda_j)|j-i|^{\beta}, \tag{5}$$

with adjustable parameter $\beta = -1$.[46] In general, λ_{SHD} increases with increasing mean hydrophobicity, $\langle\lambda\rangle$, and when the hydrophobic residues are spatially clustered in a sequence. Indeed, we found that both λ_{SHD} and $\langle\lambda\rangle$ increased monotonically with increasing number of aromatic residues (Table 1). Note that the spatial distribution of charged residues is identical for all variants with a patterning parameter[21] of 0.215, and that all protein chains have a net positive charge of $Q = \sum_i^N q_i = 8\,\mathrm{e}$.

Table 1: Sequence hydropathy decoration parameter, λ_{SHD}, mean hydrophobicity, $\langle\lambda\rangle$, of the four investigated variants of A1-LCD.

Variant	λ_{SHD}	$\langle\lambda\rangle$
Aro^{+}	5.58	0.62
WT	5.48	0.61
Aro^{-}	5.33	0.59
Aro^{--}	5.18	0.57

3.1 Chain conformations

To determine the conformations of the A1-LCD variants, we performed simulations in dilute as well as concentrated solutions, and computed the radius of gyration tensor for each chain

$$\mathbf{G} = \frac{1}{M}\sum_{i}^{N} m_i \Delta\mathbf{r}_i \Delta\mathbf{r}_i^{\mathrm{T}}, \tag{6}$$

where M is the total mass of a protein chain, and $\Delta\mathbf{r}_i$ is the position of monomer i relative to the polymer's center-of-mass. The root mean square radius of gyration was taken as $R_{\mathrm{g}} \equiv \langle G_{xx} + G_{yy} + G_{zz}\rangle^{1/2}$, which is shown in Fig. 1(a) at various temperatures. At infinite

dilution, R_g increased monotonically with increasing temperature, indicating an improvement of the (effective) solvent quality. Further, IDPs with more aromatic residues had a smaller R_g at any given temperature, indicating a stronger hydrophobicity of those variants, consistent with their values of λ_{SHD} and $\langle\lambda\rangle$ (Table 1). This behavior is in semi-quantitative agreement with recent small-angle X-ray measurements of the investigated A1-LCD variants,[39] which established a decrease from $R_g \approx 2.9\,\mathrm{nm}$ (Aro^{--}) to $R_g \approx 2.4\,\mathrm{nm}$ (Aro^{+}) as the number of aromatic residues in the A1-LCD sequence was increased at $T = 296\,\mathrm{K}$ [Fig. 1(b)]. Note that even at the highest investigated temperature, the protein chains are much more compact than a self-avoiding heteropolymer of the same contour length in a good solvent, which has $R_g \approx 4.1\,\mathrm{nm}$.

It is tempting to estimate the θ-temperature T_θ of the A1-LCD variants, *i.e.*, the temperature where the attraction between the amino acids exactly cancels the polymer-swelling due to excluded volume and charge effects, by comparing the R_g data from our simulations to the theoretical value of an ideal chain, $R_{g,id} = r_0[(N-1)/6]^{1/2} \approx 1.8\,\mathrm{nm}$. This approach suggests $T_\theta \approx 200\,\mathrm{K}$ for the wild-type, and slightly lower/higher T_θ for variants with fewer/more aromatic residues. These estimates of T_θ based on single-chain statistics are, however, unreliable as one would expect that the protein chains follow ideal chain statistics at $T \approx T_\theta$ *independent* of polymer concentration,[48] which is not the case here [Fig. 1(a)]. Further, we expect from Flory-Huggins theory that T_θ should lie *above* the critical temperature T_c for a polymer solution with an upper critical solution temperature,[48,49] but this condition is not fulfilled either ($T_c \approx 291\,\mathrm{K}$, see Sec. 3.2). Thus, we advise caution against inferring the phase behavior of heteropolymers from single-chain simulations.

We also characterized the chain conformations in highly concentrated solutions ($\rho_m = 400\,\mathrm{mg/mL}$ and $800\,\mathrm{mg/mL}$) at the corresponding phase coexistence temperatures (see Sec. 3.2). Figure 1(a) shows the R_g values of these systems, which are consistently *larger* than $R_{g,id}$ and R_g of the corresponding protein chains at infinite dilution at the same temperature T. This behavior differs strongly from that of homopolymers, where one expects

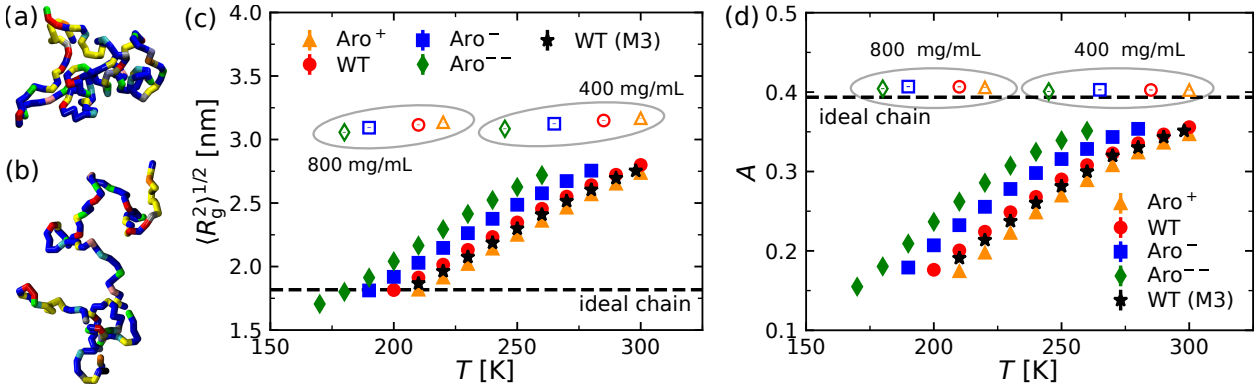

Figure 1: (a, b) Simulation snapshots of A1-LCD (WT) chains in dilute solution at (a) $T = 200\,\mathrm{K}$ and (b) $T = 300\,\mathrm{K}$. Colors indicate the different amino acid types. (c) Root mean square radius of gyration R_g and (d) relative shape asymmetry parameter A of the simulated A1-LCD variants as functions of temperature T. In both panels, filled and open symbols show results from single chain and bulk simulations, respectively. The data indicated by black stars have been computed from simulations using model M3 from Ref. 20. The horizontal dashed lines in (c) and (d) indicate the values of R_g and A for an ideal chain with the same contour length as A1-LCD.

$R_\mathrm{g} \to R_\mathrm{g,id}$ with increasing polymer concentration, either by expansion of collapsed globules (poor solvents) or by the contraction of swollen coils (good solvents) due to the screening of excluded volume interactions.[48,50] These fundamental differences ultimately stem from the fact that Flory's ideality hypothesis[50] cannot be applied to heteropolymers (see also the analysis of intermolecular contacts in Sec. 3.3).

To quantify the shape of the protein chains, we computed their relative shape asymmetry[51]

$$A = \left\langle 1 - 3\frac{G_1G_2 + G_1G_3 + G_2G_3}{(G_1 + G_2 + G_3)^2} \right\rangle \tag{7}$$

where G_1, G_2, and G_3 are the three eigenvalues of $\mathbf{G}$. The parameter A is bounded between 0 and 1, which correspond to a perfect sphere and an infinitely thin rod, respectively. The asymmetry of a three-dimensional random walk with $N \to \infty$ has been determined numerically as $A = 0.39 \pm 0.004$,[51] which reflects its strong conformational fluctuations. The protein chains are much more spherical at infinite dilution compared to an ideal chain [Fig. 1(b)], likely due to the intramolecular attraction between the hydrophobic residues of the protein chains. This hypothesis is corroborated by the fact that A1-LCD variants with

more aromatic residues have distinctly smaller A values at a given temperature T, and A approaches the value of an ideal chain with increasing T. In concentrated solutions, the shape asymmetry of the protein chains is $A \approx 0.40$ for all investigated systems [Fig. 1(b)], indicating that the chains have the shape asymmetry of a random walk.

To investigate the conformation of the IDPs in more detail, we computed the probability distributions P of the root mean square end-to-end distance, $R_{\mathrm{ee}} \equiv \langle R_{\mathrm{ee}}^2 \rangle^{1/2}$, which are shown in Fig. 2 for the single chain simulations of the wild-type. The probability distributions broaden with increasing temperature, while the position of their maximum shifts to larger R_{ee}. We have also calculated analytically $P(R_{\mathrm{ee}})$ for an ideal chain of the same contour length as A1-LCD to establish a reference point (Fig. 2).[48] The theoretical curve lies between the simulation results of the wild-type at $T = 210\,\mathrm{K}$ and $220\,\mathrm{K}$, suggesting $T_\theta \approx 215\,\mathrm{K}$, which is about $15\,\mathrm{K}$ higher than our previous estimate based on R_{g} but still far below T_{c}. Further, the $P(R_{\mathrm{ee}})$ distributions of A1-LCD are much more narrow at all investigated temperatures than $P(R_{\mathrm{ee}})$ of a heteropolymer in a good solvent.

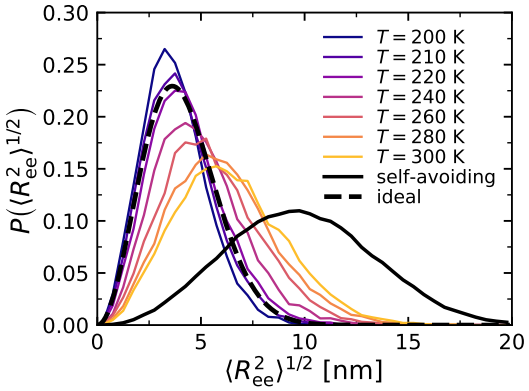

Figure 2: Probability distribution P of the end-to-end distance, R_{ee}, from single chain simulations of A1-LCD (WT) for different temperatures (solid colored lines). Data for an ideal[48] and a self-avoiding chain with the same contour lengths as A1-LCD are included as dashed and solid black lines, respectively.

We have also calculated the mean interresidue distances, $\langle (\mathbf{r}_i - \mathbf{r}_j)^2 \rangle^{1/2}$, which are shown in Fig. 3 for A1-LCD (WT) at various temperatures. These data show that the A1-LCD (WT) chains are locally more swollen than ideal chains due to excluded volume effects

between nearby residues, but are much more compact than a self-avoiding heteropolymer in a good solvent. Our analysis of the chain conformations clearly demonstrates that there is *no single* temperature where the A1-LCD protein chains follow the statistics of an ideal or self-avoiding polymer; instead, there is a rather broad temperature range where certain properties agree but other ones deviate. These differences are rooted in the heterogeneous nature of protein chains, which makes it impossible to describe them—even at high degree of coarse-graining—as self-similar fractal objects.

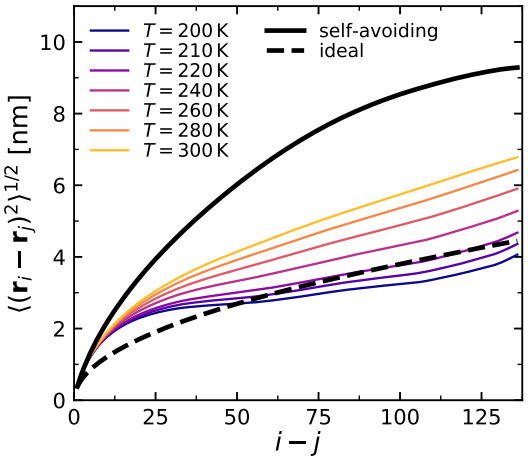

Figure 3: Mean interresidue distance $\langle(\mathbf{r}_i - \mathbf{r}_j)^2\rangle^{1/2}$ from single chain simulations of A1-LCD (WT) at various temperatures. Data for an ideal and a self-avoiding chain with the same contour lengths as A1-LCD are included as dashed and solid black lines, respectively.

3.2 Phase behavior

We determined the vapor-liquid phase coexistence densities of the protein chains from MD simulations containing both a low density vapor phase and a high density liquid phase in the same (elongated) simulation box.[15,52,53] Initially, the chains were placed in a densely packed slab, with its two surface normals lying parallel to the z-axis. The dimensions of the simulation box ($L_x = L_y = 15\,\text{nm}$ and $L_z = 75\,\text{nm}$) and the total number of chains ($N_\text{c} = 110$) were chosen such that the two vapor-liquid interfaces of the slab can be assumed as non-interacting with each other. The systems were then simulated for $10\,\mu\text{s}$. Measurements

were taken once the memory of the starting configuration was completely lost (typically after $t = 1\,\mu$s), which we verified by tracking R_g as well as the densities in the liquid and vapor regions. Figures 4(a-c) show selected simulation snapshots of the A1-LCD (WT) at temperatures below and above the estimated critical temperature, $T_c \approx 291\,$K (see further below).

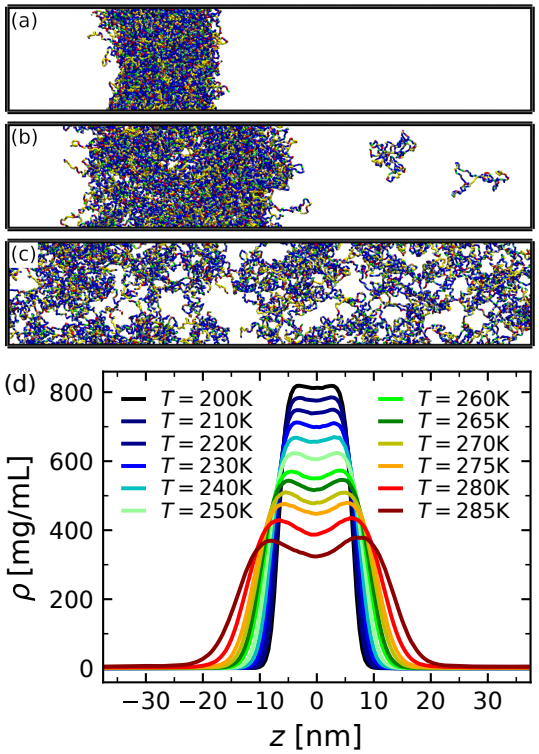

Figure 4: Simulation snapshots of A1-LCD (WT) at three selected temperatures (a) $T = 200\,$K, (b) $T = 280\,$K, and (c) $T = 320\,$K. Colors indicate the different amino acid types. (d) Density profiles obtained by simulations of 110 chains of A1-LCD (WT) for various temperatures, as indicated.

Figure 4(d) shows the corresponding density profiles for various temperatures. With increasing temperature T, the density of the vapor phase, ρ_v, increased, whereas the density of the liquid phase, ρ_l, decreased, similar to the phase behavior of homopolymers in solution.[48,52,53] Interestingly, the density profiles show microstructuring in the liquid phase, where the condensate is denser at the interface than at its center. These inhomogeneities are more pronounced at higher temperatures. The depletion of protein chains at the center of the condensates is also apparent in Fig. 4(b), where a small 'crack' is noticeable in the

condensate center. Given the net positive charge of the A1-LCD chains ($Q = 8\,\mathrm{e}$ per chain), we surmise that the intra-condensate structuring is likely due to the long-range repulsion between like-charged residues. Thus, one might expect that the positively charged residues have a tendency to face the aqueous solvent to minimize their long-range repulsion. However, we did not find such segregation, probably because the charged residues are uniformly distributed in the protein sequence. To test whether the charged residues are responsible for the microstructuring, we performed additional simulations of uncharged A1-LCD (WT) chains, and found indeed much flatter density profiles (see Supporting Information).

We determined the critical temperature T_c by fitting the density profiles from the MD simulations to

$$\Delta\rho = B(1 - T/T_\mathrm{c})^\beta \tag{8}$$

with order parameter $\Delta\rho = \rho_\mathrm{l} - \rho_\mathrm{v}$, critical amplitude B, and critical exponent $\beta = 0.325$, assuming that our systems belong to the $3d$-Ising universality class. To estimate the critical density ρ_c, we consider the rectilinear diameter ρ_d

$$\rho_\mathrm{d} = (\rho_\mathrm{l} + \rho_\mathrm{v})/2 = \rho_\mathrm{c} + C(T_\mathrm{c} - T) \tag{9}$$

with positive (fitting) constant C. We did not perform a finite-size scaling analysis of the critical behavior due to the additional computing costs, but anticipate that such systematic errors are comparable to the statistical error in determining the critical point by fitting Eq. (8).[53]

Table 2: Critical temperatures and densities from our MD simulations ($T_\mathrm{c}^\mathrm{sim}$ and $\rho_\mathrm{c}^\mathrm{sim}$) and from experiments[39] ($T_\mathrm{c}^\mathrm{exp}$ and $\rho_\mathrm{c}^\mathrm{exp}$) for investigated variants of A1-LCD.

Variant	$T_\mathrm{c}^\mathrm{sim}$ [K]	$\rho_\mathrm{c}^\mathrm{sim}$ [mg/mL]	$T_\mathrm{c}^\mathrm{exp}$ [K]	$\rho_\mathrm{c}^\mathrm{exp}$ [mg/mL]
Aro^+	310 ± 2	186 ± 30	357.75	100.9
WT	291 ± 2	181 ± 32	338.75	79.9
Aro^-	271 ± 2	205 ± 67	303.45	95.6
Aro^{--}	249 ± 1	204 ± 63	-	-

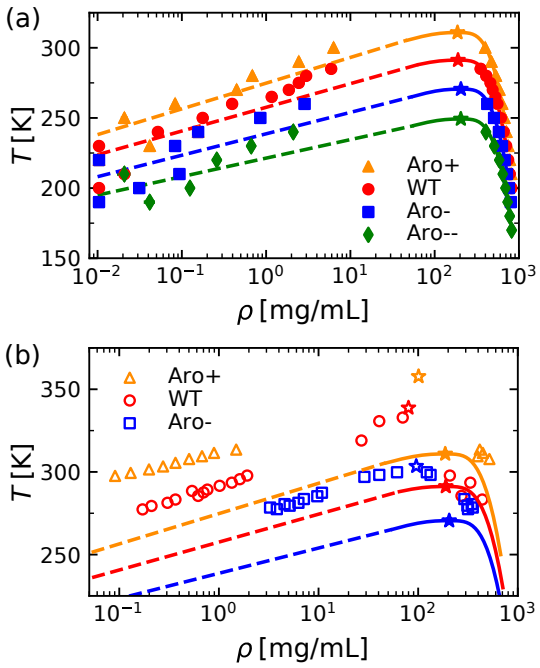

Figure 5: (a) Phase diagrams of the A1-LCD variants from simulations. Symbols show coexisting densities from simulations, while solid lines represent the theoretical curves, obtained by fitting the simulation data to Eqs. (8) and (9). Dashed lines are guides to the eye. (b) Comparison between simulations and experiments. Lines correspond to the fitted simulation data shown in (a), while experimental data are indicated by open symbols. Critical points are indicated by stars in both panels.

Figure 5 shows the resulting phase diagrams from simulations as well as the corresponding experimental results from Ref. 39. Based on our analysis, we find that T_c increases with increasing number of aromatic residues in the protein chains, while the critical density ρ_c decreases slightly (Table 2). These trends are in semi-quantitative agreement with experimental results,[39] but T_c is about $30 - 50\,\mathrm{K}$ lower in the simulations compared to the experiments, while ρ_c is about $100\,\mathrm{mg/mL}$ larger in the simulations (see Table 2). There are several potential sources for these differences, which we will briefly discuss in the following to guide future model improvements: (i) The employed model[15] (and also its recent modification[20]) has been parameterized to match single chain conformations at infinite dilution, which does *not* guarantee correct interactions between multiple chains. Such many-body interactions could be included through local-density dependent potentials.[54,55] (ii) The IDPs are considered as fully flexible chains, and thus does not capture any secondary structures and/or

local bending rigidity, which might affect the phase behavior of the protein chains.[56–58] Such local chain structures could be included in coarse-grained models *via* Gō-type interactions parameterized through experimental data or atomistic simulations.[59–61] (iii) Electrostatic interactions between charged residues are included *via* a screened Coulomb potential [Eq. (3)] with constant dielectric constant $\epsilon_\mathrm{r} = 80$, which is a decent approximation for dilute solutions of moderately charged protein chains in water, but less accurate for inhomogeneous dielectric media. This mean-field description of the electrostatics could be improved in the future by using, *e.g.*, a generalized Born model.[62,63] (iv) Both hydrophobic and electrostatic interactions are truncated at a cutoff radius, which can have a sizable impact on the phase behavior, especially near criticality.[64] To demonstrate this effect, we ran additional simulations of A1-LCD (WT) with a smaller cutoff radius for the hydrophobic interactions ($r_\mathrm{c}^\mathrm{LJ} = 1.4\,\mathrm{nm}$ instead of $2.0\,\mathrm{nm}$), finding that T_c decreased by about $62\,\mathrm{K}$ (see Supporting Information). Nevertheless, the agreement between simulations and experiments is rather remarkable, given the heavily coarse-grained and generic nature of the employed model.

We also determined the surface tension of the protein chains, γ, from the slab simulations using the Kirkwood-Buff relation

$$\gamma = \frac{L_z}{2}\left(P_{zz} - \frac{P_{xx} + P_{yy}}{2}\right), \tag{10}$$

where the factor $1/2$ accounts for the two interfaces present in the system. The components of the pressure tensor, $P_{\alpha\beta}$, are calculated *via* the standard Clausius virial equation. Figure 6 shows the temperature-dependence of γ, which goes to zero as $T \to T_\mathrm{c}$, as expected. At fixed T, protein chains containing more aromatic residues have larger γ [Fig. 6(a)], which is consistent with their overall higher hydrophobicity (Table 1). For biologically relevant protein concentrations in the range of $\rho \approx 400 - 800\,\mathrm{mg/mL}$ (simulated at the corresponding phase coexistence temperatures far from criticality, *cf.* Fig. 5), the computed surface tensions lied between $5\,\mu\mathrm{N/m}$ and $800\,\mu\mathrm{N/m}$, which is comparable to recent experimental

measurements of phase separated protein droplets.[65–67] A similar range of $\gamma \approx 15-380\,\mu$N/m was also measured for fused in sarcoma (FUS) proteins in recent MD simulations, using a very different coarse-grained model with an explicit solvent.[18] Interestingly, these values are several orders of magnitude smaller than typical interfacial tensions of simple liquid combinations, *e.g.*, alkane droplets in water which have $\gamma \approx 50\,$mN/m at room temperature.[68,69] One might speculate that the comparatively lower surface tensions found in simulations and experiments of condensed IDPs, such as hnRNPA1 and the related protein FUS, stem from their large fraction of hydrophilic and only weakly hydrophobic residues. For instance, in the sticker and spacer representation of A1-LCD (WT) employed by Martin *et al.*,[39] only about 15 % of residues were selected as hydrophobic stickers, which is in qualitative agreement with our contact map analysis (see Sec. 3.3 below). Indeed, simulations of highly hydrophobic Phenylalanine or Proline homopolymer chains give much larger surface tensions for the same temperature range, *e.g.*, $\gamma \approx 7\,$mN/m for Phenylalanine at room temperature (see Supporting Information).

Finally, we can use the surface tension data from our simulations to verify the postulated compatibility with the $3d$-Ising universality class, for which one expects $\gamma = \gamma_0(1 - T/T_\mathrm{c})^\mu$ near the critical point, with amplitude γ_0 and critical exponent $\mu \approx 1.26$.[70] We found $\mu = 1.18 \pm 0.32$ when fitting our simulation data in the range $1 - T/T_\mathrm{c} \leq 0.20$, which is in decent agreement with the theoretically expected value [Fif. 6(b)]. Further, γ_0 increased with increasing number of aromatic residues in the protein chains.

3.3 Contact Maps

To determine the inter-chain contacts of the IDPs in the concentrated regime, we performed additional bulk simulations at $\rho = 400\,$mg/mL and $800\,$mg/mL for all four variants (WT, Aro$^-$, Aro^{--}, and Aro$^+$). The temperature of each simulation was set to the calculated coexistence temperature (Fig. 5). Intermolecular contacts can be identified through, *e.g.*, distance-[15] or energy-based[20] metrics. Appropriate criteria can be easily defined in lattice-

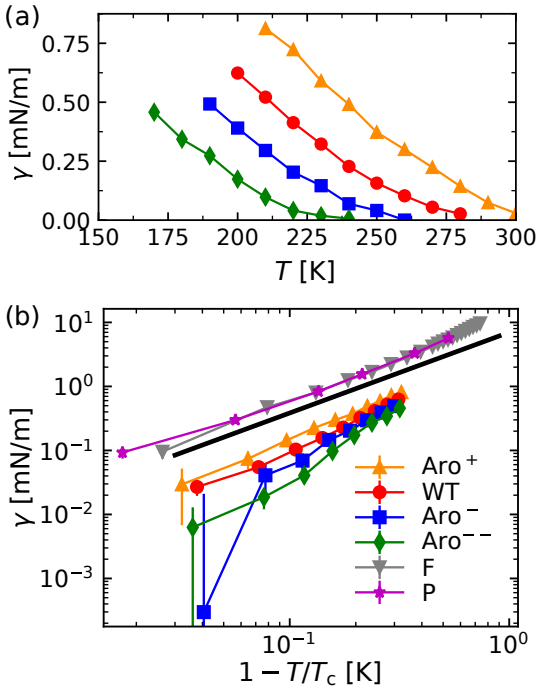

Figure 6: Surface tension of the protein chains as functions of (a) T and (b) $1-T/T_c$. In panel (b), the black line indicates the theoretically expected scaling for the $3d$-Ising universality class, $\gamma \propto (1-T/T_c)^{1.26}$.

based simulations,[39] due to their inherently discretized length- and energy-scales. In off-lattice simulations (and also experimental systems) there is, however, some ambiguity in defining intermolecular contacts. Typically, distance-based metrics count the number of pairs within a specified cutoff radius r_c^{ij},[15] while energy-based criteria consider pairwise interaction energies.[20] We studied the intermolecular contacts using both methods. To establish a baseline reference, we also performed additional simulations of self-avoiding heteropolymers under good solvent conditions for all residues.

In accordance with the trends from simulations of single chains (see Sec. 3.1) and the phase behavior of the A1-LCD variants (see Sec. 3.2), we find that aromatic residues engage in many important interactions. Figure 7(a) shows the intermolecular contact map for all residues of A1-LCD (WT) at $\rho = 400\,\mathrm{mg/mL}$, using a distance-based metric where two residues are in contact when their distance is below $1.1 \times 2^{1/6}\,\sigma_{ij}$. Inter-chain contacts are distributed uniformly along the protein sequence, where residues that form many contacts,

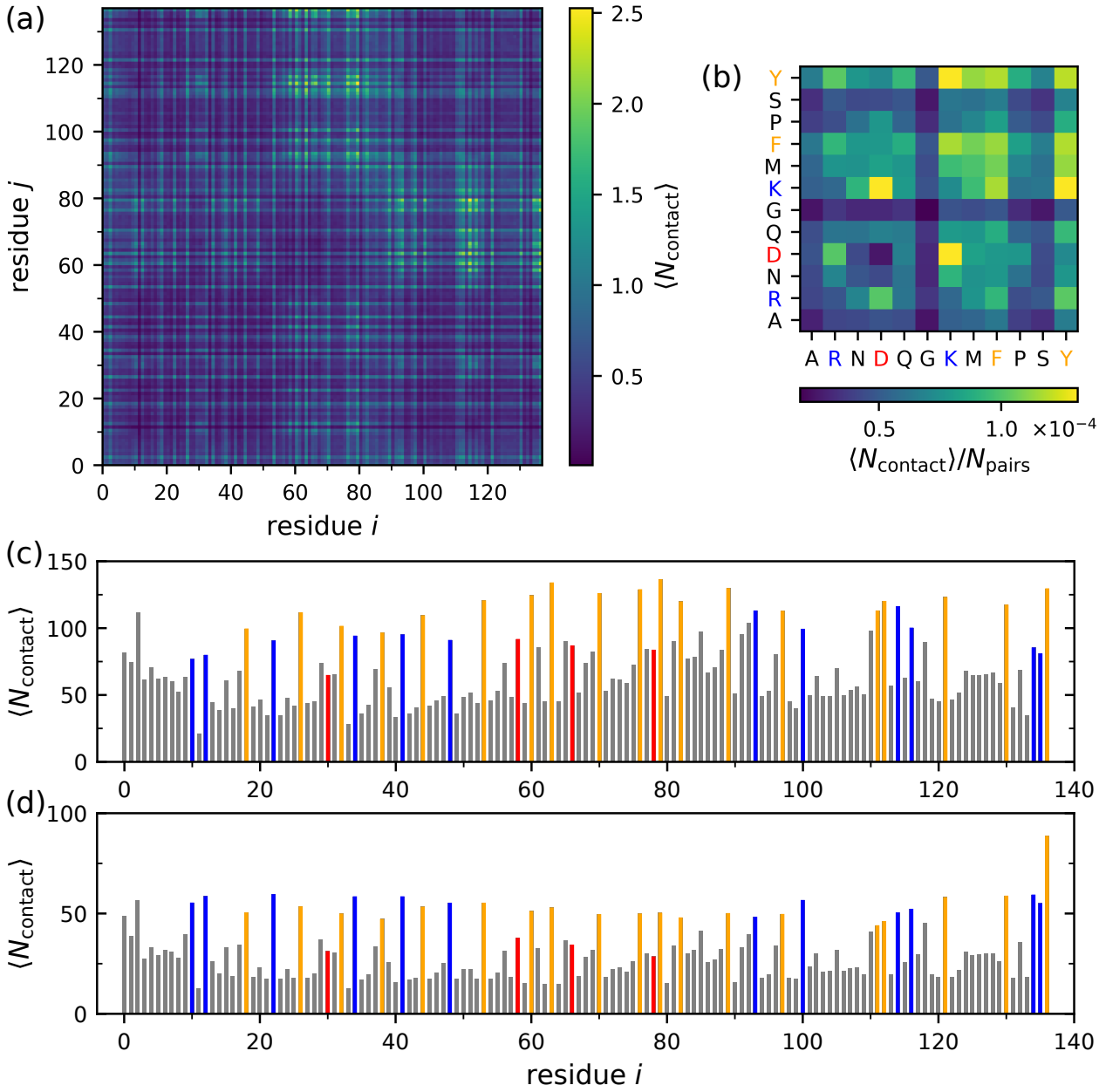

Figure 7: Distance-based contact maps for A1-LCD (WT) at $\rho = 400\,\mathrm{mg/mL}$ and $T = 285\,\mathrm{K}$. (a) Average number of intermolecular contacts for a pair of residues i and j. (b) Average number of intermolecular contacts based on type, normalized by the corresponding number of possible interaction pairs, N_{pairs}. (c) 1D-projection of residual contact map. (d) Same as (c) but for a heteropolymer in a good solvent. (c,d) Aromatic residues (F and Y) are marked in orange, negatively charged residues (D) are marked in red, while positively charged ones (R and K) are shown in blue.

whether charged or aromatic, are typically followed by residues that do not engage in many contacts. To better see which residue types predominantly form contacts, we reduce the full contact map by summing over all entries with the same type of pairs, and then divide the sum by the number of possible interaction partners for each pair of types, N_{pair}. The resulting data is shown in Fig. 7(b), highlighting that contacts between hydrophobic residues K, F, M, and Y are among the most prominent intermolecular contacts formed in the simulations of A1-LCD condensates. In contrast, A, G, and P residues have much fewer contacts although they have similar hydrophobicity parameters λ_i (see Supporting Information). Charged residues R, K, and D also form distinct contacts with their oppositely charged partners. Simulation of a purely repulsive reference system of uncharged A1-LCD (WT) chains shows that aromatic residues F and Y still form many contacts [Fig. 7(d)], which is likely due to the larger sizes of F and Y residues; this may be explain why these residue types are typically more important stickers than smaller hydrophobic residues, such as A, G, and P. The comparison with the purely repulsive reference simulation also highlights the contacts between positively and negatively charged R-D and K-D pairs.

Computing the intermolecular interaction energies provides an alternative perspective on the contact pair formation. Figures 8(a,b) show the contributions from van der Waals and electrostatic interactions, demonstrating that both aromatic and charged residues engage in stabilizing interactions, and can thus be considered as stickers. In particular, M, F, P, and Y residues are strongly attracted to each other, which reflects their high hydrophobicity.[15] According to Fig. 8(b), R-Y interactions are favorable but less favorable than Y-Y contacts , which may require modifications of the parameter set to capture experimentally-observed R-Y attraction.[32] Considering electrostatic interactions, the negatively charged D residues are highly attracted to the positively charged R and K residues, while interactions between like-charged residues are unfavorable, as expected. Overall, electrostatic interactions are about one order of magnitude stronger than van der Waals interactions, so that two like-charged residues still repel each other even if they are highly hydrophobic. As the IDPs feature

an excess of positively charged residues, it is not surprising that the negatively charged D residues engage in favorable charge-charge interactions. Recent work has highlighted that charged residues can also be important "stickers" in agreement with our results.[40]

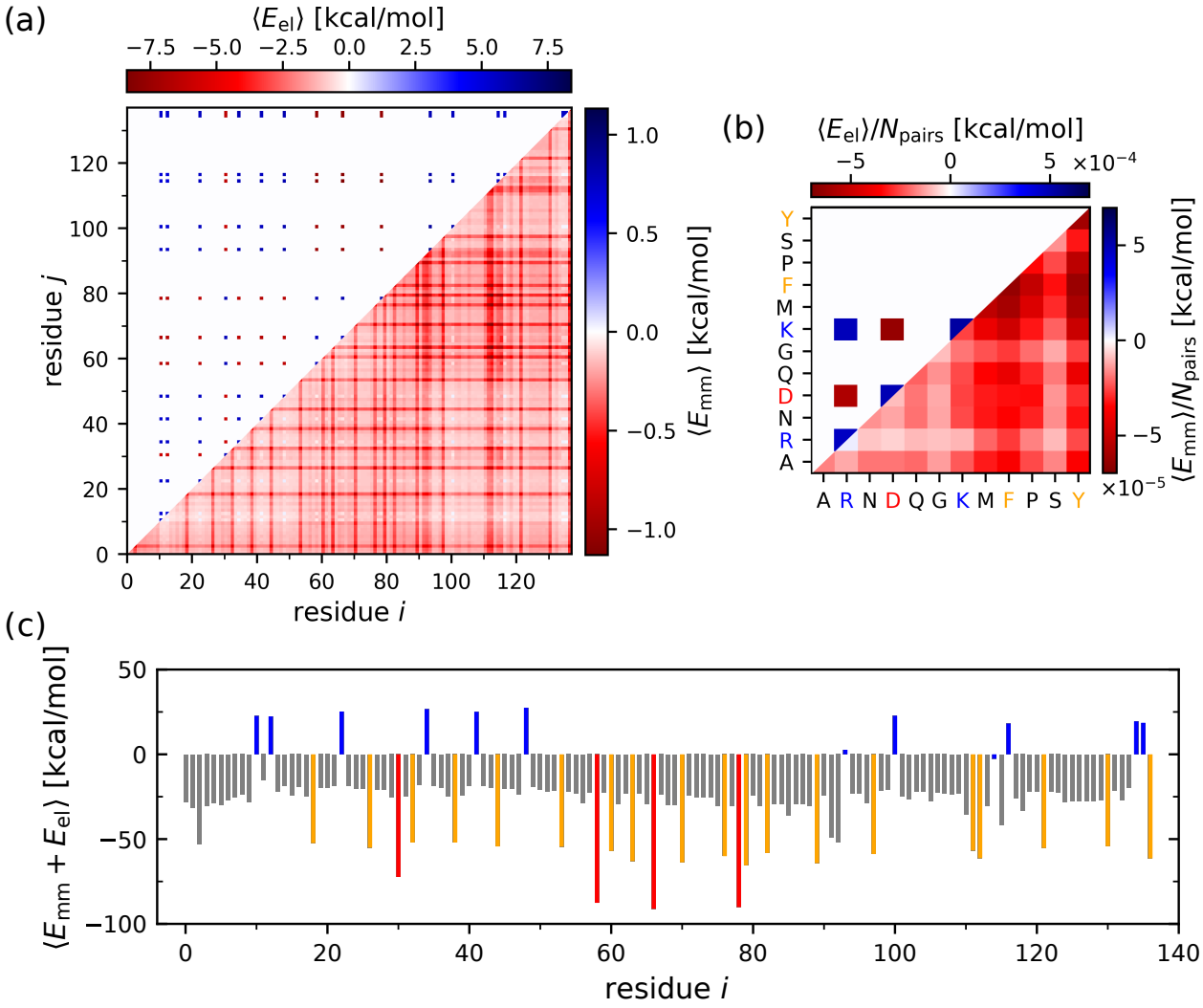

Figure 8: Energy-based contact maps for A1-LCD (WT) at $\rho = 400\,\mathrm{mg/mL}$ and $T = 285\,\mathrm{K}$. (a) Intermolecular monomer-monomer interaction energies, and (b) normalized interaction energies per type, split into electrostatic (top left half) and van der Waals interactions (bottom right half). (c) 1D-projection of interaction energies. Aromatic residues are marked in orange, charged residues are marked in red (negative) and blue (positive).

4 Conclusions

We have investigated the conformation and phase behavior of A1-LCD protein chains in the dilute and condensed state through molecular simulations. We investigated the wild-type as well as three mutated variants with fewer or more aromatic residues, and compared our simulations with recent experiments. Even at a relatively coarse-grained representation, with one bead per amino acid and an implicit solvent, we observed rich behavior of A1-LCD proteins and identified important trends: In dilute solutions, chains with more aromatic residues in their sequence were more compact and more spherical. In condensates, the chains were much more extended, with similar chain conformations for the different variants. These findings are particularly interesting in light of recent experiments that have also observed differences in protein chain conformations between dilute and dense phases: For example, recent single-molecule Förster resonance energy transfer experiments revealed that the intrinsically disordered protein Tau, which is implicated in neurodegenerative diseases such as Alzheimer's disease, expands in condensates.[14] In contrast, magnetic resonance experiments found a compaction of the fused in sarcoma protein in condensates.[13]

Further, we observed that the critical temperature of the phase-separated systems increased with increasing number of aromatic residues in the sequence. To elucidate this behavior, we carried out a distance- and energy-based contact analysis, revealing that charged and aromatic residues form the majority of intermolecular contacts. We also found distinct micro-structuring in the liquid phase near criticality, driven by electrostatics, which may also occur in other condensates of charged proteins.[40] Our simulations also revealed that the phase-separated condensates have distinctly smaller surface tensions than typical combinations of immiscible simple liquids, such as alkane droplets in water, which we attribute to the large fraction of hydrophilic residues in the protein sequences. In general, we found that the heterogeneous nature of the protein sequence, with different hydrophobic, polar, and charged amino acids, makes it difficult to apply standard homopolymer models even at the employed level of coarse-graining.

Supporting Information

Protein sequences and additional simulation details; additional contact maps, phase diagrams, and surface tension data

Notes

The authors declare no competing financial interest.

Acknowledgments

We thank Prof. Alex S. Holehouse for fruitful discussions. This work was supported by the Deutsche Forschungsgemeinschaft (DFG, German Research Foundation) through Project Nos. 274340645, 405552959, and 470113688. D.J.B. acknowledges support through the Max Planck Graduate Center with the Johannes Gutenberg University Mainz (MPGC). L.S.S. acknowledges support by ReALity (Resilience, Adaptation and Longevity), M^{3}ODEL and Forschungsinitiative des Landes Rheinland-Pfalz. The authors gratefully acknowledge the computing time granted on the supercomputer Mogon (hpc.uni-mainz.de).

References

(1) Brangwynne, C. P.; Eckmann, C. R.; Courson, D. S.; Rybarska, A.; Hoege, C.; Gharakhani, J.; Jülicher, F.; Hyman, A. A. Germline P Granules Are Liquid Droplets That Localize by Controlled Dissolution/Condensation. *Science* **2009**, *324*, 1729 LP – 1732.

(2) Hyman, A. A.; Weber, C. A.; Jülicher, F. Liquid-Liquid Phase Separation in Biology. *Annu. Rev. Cell Dev. Biol.* **2014**, *30*, 39–58.

(3) Wang, J.; Choi, J. M.; Holehouse, A. S.; Lee, H. O.; Zhang, X.; Jahnel, M.; Maharana, S.; Lemaitre, R.; Pozniakovsky, A.; Drechsel, D.; Poser, I.; Pappu, R. V.; Alberti, S.; Hyman, A. A. A Molecular Grammar Governing the Driving Forces for Phase Separation of Prion-like RNA Binding Proteins. *Cell* **2018**,

(4) Jawerth, L.; Fischer-Friedrich, E.; Saha, S.; Wang, J.; Franzmann, T.; Zhang, X.; Sachweh, J.; Ruer, M.; Ijavi, M.; Saha, S.; Mahamid, J.; Hyman, A. A.; Jülicher, F. Protein condensates as aging Maxwell fluids. *Science* **2020**, *370*, 1317–1323.

(5) Hofweber, M.; Hutten, S.; Bourgeois, B.; Spreitzer, E.; Niedner-Boblenz, A.; Schifferer, M.; Ruepp, M.-D.; Simons, M.; Niessing, D.; Madl, T.; Dormann, D. Phase Separation of FUS Is Suppressed by Its Nuclear Import Receptor and Arginine Methylation. *Cell* **2018**, *173*, 706–719.e13.

(6) Alberti, S.; Hyman, A. A. Are aberrant phase transitions a driver of cellular aging? *BioEssays* **2016**, *38*, 959–968.

(7) Gruijs da Silva, L. A.; Simonetti, F.; Hutten, S.; Riemenschneider, H.; Sternburg, E. L.; Pietrek, L. M.; Gebel, J.; Dötsch, V.; Edbauer, D.; Hummer, G.; Stelzl, L. S.; Dormann, D. Disease-linked TDP-43 hyperphosphorylation suppresses TDP-43 condensation and aggregation. *EMBO J. n/a*, e108443.

(8) Portz, B.; Lee, B. L.; Shorter, J. FUS and TDP-43 Phases in Health and Disease. *Trends Biochem. Sci.* **2021**, *46*, 550–563.

(9) Kar, M.; Dar, F.; Welsh, T. J.; Vogel, L.; Kühnemuth, R.; Majumdar, A.; Krainer, G.; Franzmann, T. M.; Alberti, S.; Seidel, C. A. M.; Knowles, T. P.; Hyman, A. A.; Pappu, R. V. Phase separating RNA binding proteins form heterogeneous distributions of clusters in subsaturated solutions. *bioRxiv* **2022**,

(10) Burke, K. A.; Janke, A. M.; Rhine, C. L.; Fawzi, N. L. Residue-by-Residue View of In

Vitro FUS Granules that Bind the C-Terminal Domain of RNA Polymerase II. *Mol. Cell* **2015**, *60*, 231–241.

(11) Brady, J. P.; Farber, P. J.; Sekhar, A.; Lin, Y.-H.; Huang, R.; Bah, A.; Nott, T. J.; Chan, H. S.; Baldwin, A. J.; Forman-Kay, J. D.; Kay, L. E. Structural and hydrodynamic properties of an intrinsically disordered region of a germ cell-specific protein on phase separation. *Proc. Natl. Acad. Sci. U. S. A.* **2017**, *114*, E8194–E8203.

(12) Murthy, A. C.; Dignon, G. L.; Kan, Y.; Zerze, G. H.; Parekh, S. H.; Mittal, J.; Fawzi, N. L. Molecular interactions underlying liquid-liquid phase separation of the FUS low-complexity domain. *Nat. Struct. Mol. Biol.* **2019**, *26*, 637–648.

(13) Emmanouilidis, L.; Esteban-Hofer, L.; Damberger, F. F.; de Vries, T.; Nguyen, C. K. X.; Ibáñez, L. F.; Mergenthal, S.; Klotzsch, E.; Yulikov, M.; Jeschke, G.; Allain, F. H. T. NMR and EPR reveal a compaction of the RNA-binding protein FUS upon droplet formation. *Nat. Chem. Biol.* **2021**, *17*, 608–614.

(14) Wen, J.; Hong, L.; Krainer, G.; Yao, Q.-Q.; Knowles, T. P. J.; Wu, S.; Perrett, S. Conformational Expansion of Tau in Condensates Promotes Irreversible Aggregation. *J. Am. Chem. Soc.* **2021**, *143*, 13056–13064, PMID: 34374536.

(15) Dignon, G. L.; Zheng, W.; Kim, Y. C.; Best, R. B.; Mittal, J. Sequence determinants of protein phase behavior from a coarse-grained model. *PLoS Comput. Biol.* **2018**, *14*, e1005941.

(16) Paloni, M.; Bailly, R.; Ciandrini, L.; Barducci, A. Unraveling Molecular Interactions in Liquid–Liquid Phase Separation of Disordered Proteins by Atomistic Simulations. *J. Phys. Chem. B* **2020**, *124*, 9009–9016.

(17) Espinosa, J. R.; Joseph, J. A.; Sanchez-Burgos, I.; Garaizar, A.; Frenkel, D.; Collepardo-Guevara, R. Liquid network connectivity regulates the stability and composition of biomolecular condensates with many components. *Proc. Natl. Acad. Sci. U. S. A.* **2020**,

(18) Benayad, Z.; von Bülow, S.; Stelzl, L. S.; Hummer, G. Simulation of FUS Protein Condensates with an Adapted Coarse-Grained Model. *J. Chem. Theory Comput.* **2021**, *17*, 525–537.

(19) Latham, A. P.; Zhang, B. Consistent Force Field Captures Homologue-Resolved HP1 Phase Separation. *J. Chem. Theory Comput.* **2021**, *17*, 3134–3144.

(20) Tesei, G.; Schulze, T. K.; Crehuet, R.; Lindorff-Larsen, K. Accurate model of liquid–liquid phase behavior of intrinsically disordered proteins from optimization of single-chain properties. *Proc. Natl. Acad. Sci. U. S. A.* **2021**, *118*, e2111696118.

(21) Das, R. K.; Pappu, R. V. Conformations of intrinsically disordered proteins are influenced by linear sequence distributions of oppositely charged residues. *Proc. Natl. Acad. Sci. U. S. A.* **2013**, *110*, 13392–13397.

(22) Stelzl, L. S.; Pietrek, L. M.; Holla, A.; Oroz, J.; Sikora, M.; Köfinger, J.; Schuler, B.; Zweckstetter, M.; Hummer, G. Global Structure of the Intrinsically Disordered Protein Tau Emerges from Its Local Structure. *JACS Au 2*, 673–686.

(23) Dignon, G. L.; Zheng, W.; Best, R. B.; Kim, Y. C.; Mittal, J. Relation between single-molecule properties and phase behavior of intrinsically disordered proteins. *Proc. Natl. Acad. Sci. U. S. A.* **2018**, *115*, 9929–9934.

(24) Jin, F.; Gräter, F. How multisite phosphorylation impacts the conformations of intrinsically disordered proteins. *PLoS Comput. Biol.* **2021**, *17*, e1008939.

(25) Martin, E. W.; Holehouse, A. S.; Grace, C. R.; Hughes, A.; Pappu, R. V.; Mittag, T. Sequence Determinants of the Conformational Properties of an Intrinsically Disordered Protein Prior to and upon Multisite Phosphorylation. *J. Am. Chem. Soc.* **2016**, *138*, 15323–15335.

(26) Zheng, W.; Dignon, G. L.; Jovic, N.; Xu, X.; Regy, R. M.; Fawzi, N. L.; Kim, Y. C.; Best, R. B.; Mittal, J. Molecular Details of Protein Condensates Probed by Microsecond Long Atomistic Simulations. *J. Phys. Chem. B* **2020**, *124*, 11671–11679, PMID: 33302617.

(27) Peter, C.; Kremer, K. Multiscale simulation of soft matter systems – from the atomistic to the coarse-grained level and back. *Soft Matter* **2009**, *5*, 4357.

(28) Ghavami, A.; van der Giessen, E.; Onck, P. R. Coarse-Grained Potentials for Local Interactions in Unfolded Proteins. *J. Chem. Theory Comput.* **2013**, *9*, 432–440.

(29) Ruff, K. M.; Harmon, T. S.; Pappu, R. V. CAMELOT: A machine learning approach for coarse-grained simulations of aggregation of block-copolymeric protein sequences. *J. Chem. Phys.* **2015**, *143*, 243123.

(30) Choi, J.-M.; Dar, F.; Pappu, R. V. LASSI: A lattice model for simulating phase transitions of multivalent proteins. *PLoS Comput. Biol.* **2019**, *15*, e1007028.

(31) Dignon, G. L.; Zheng, W.; Kim, Y. C.; Mittal, J. Temperature-Controlled Liquid–Liquid Phase Separation of Disordered Proteins. *ACS Cent. Sci.* **2019**, *5*, 821–830.

(32) Das, S.; Lin, Y.-H.; Vernon, R. M.; Forman-Kay, J. D.; Chan, H. S. Comparative roles of charge, π, and hydrophobic interactions in sequence-dependent phase separation of intrinsically disordered proteins. *Proc. Natl. Acad. Sci. U. S. A.* **2020**, *117*, 28795–28805.

(33) Regy, R. M.; Thompson, J.; Kim, Y. C.; Mittal, J. Improved coarse-grained model for studying sequence dependent phase separation of disordered proteins. *Protein Sci.* **2021**, *30*, 1371–1379.

(34) Winnik, M. A.; Yekta, A. Associative polymers in aqueous solution. *Curr. Opin. Colloid Interface Sci.* **1997**, *2*, 424–436.

(35) Feric, M.; Vaidya, N.; Harmon, T. S.; Mitrea, D. M.; Zhu, L.; Richardson, T. M.; Kriwacki, R. W.; Pappu, R. V.; Brangwynne, C. P. Coexisting liquid phases underlie nucleolar subcompartments. *Cell* **2016**, *165*, 1686–1697.

(36) Choi, J.-M.; Holehouse, A. S.; Pappu, R. V. Physical Principles Underlying the Complex Biology of Intracellular Phase Transitions. *Annu. Rev. Biophys.* **2020**, *49*, 107–133.

(37) Theillet, F.-X.; Kalmar, L.; Tompa, P.; Han, K.-H.; Selenko, P.; Dunker, A. K.; Daughdrill, G. W.; Uversky, V. N. The alphabet of intrinsic disorder: I. Act like a Pro: On the abundance and roles of proline residues in intrinsically disordered proteins. *Intrinsically Disord. Proteins* **2013**, *1*, e24360.

(38) Lichtinger, S. M.; Garaizar, A.; Collepardo-Guevara, R.; Reinhardt, A. Targeted modulation of protein liquid-liquid phase separation by evolution of amino-acid sequence. *PLOS Comput. Biol.* **2021**, *17*, e1009328.

(39) Martin, E. W.; Holehouse, A. S.; Peran, I.; Farag, M.; Incicco, J. J.; Bremer, A.; Grace, C. R.; Soranno, A.; Pappu, R. V.; Mittag, T. Valence and patterning of aromatic residues determine the phase behavior of prion-like domains. *Science* **2020**, *367*, 694–699.

(40) Bremer, A.; Farag, M.; Borcherds, W. M.; Peran, I.; Martin, E. W.; Pappu, R. V.; Mittag, T. Deciphering how naturally occurring sequence features impact the phase behaviours of disordered prion-like domains. *Nat. Chem.* **2022**, *14*, 196–207.

(41) Kapcha, L. H.; Rossky, P. J. A Simple Atomic-Level Hydrophobicity Scale Reveals Protein Interfacial Structure. *J. Mol. Biol.* **2014**, *426*, 484–498.

(42) Anderson, J. A.; Glaser, J.; Glotzer, S. C. HOOMD-blue: A Python Package for High-Performance Molecular Dynamics and Hard Particle Monte Carlo Simulations. *Comput. Mater. Sci.* **2020**, *173*, 109363.

(43) https://github.com/mphowardlab/azplugins.

(44) Humphrey, W.; Dalke, A.; Schulten, K. VMD - Visual Molecular Dynamics. *J. Molec. Graphics* **1996**, *14*, 33–38.

(45) Statt, A.; Casademunt, H.; Brangwynne, C. P.; Panagiotopoulos, A. Z. Model for disordered proteins with strongly sequence-dependent liquid phase behavior. *J. Chem. Phys.* **2020**, *152*, 075101.

(46) Zheng, W.; Dignon, G. L.; Brown, M.; Kim, Y. C.; Mittal, J. Hydropathy Patterning Complements Charge Patterning to Describe Conformational Preferences of Disordered Proteins. *J. Phys. Chem. Lett.* **2020**, *11*, 3408–3415.

(47) Webb, M. A.; Jackson, N. E.; Gil, P. S.; de Pablo, J. J. Model for disordered proteins with strongly sequence-dependent liquid phase behavior. *Sci. Adv.* **2020**, *6*, eabc6216.

(48) Rubinstein, M.; Colby, R. H. *Polymer Physics*; Oxford University Press, Oxford, 2003.

(49) Schultz, A. R.; Flory, P. J. Phase Equilibria in Polymer-Solvent Systems. *J. Am. Chem. Soc.* **1952**, *74*, 4760–4767.

(50) Flory, P. J. *Statistical mechanics of chain molecules*; Oxford University Press, New York, 1988.

(51) Rudnick, J.; Gaspari, G. The Shapes of Random Walks. *Science* **1987**, *237*, 384–389.

(52) Silmore, K. S.; Howard, M. P.; Panagiotopoulos, A. Z. Vapour–liquid phase equilibrium and surface tension of fully flexible Lennard–Jones chains. *Mol. Phys.* **2017**, *115*, 320–327.

(53) Midya, J.; Egorov, S. A.; Binder, K.; Nikoubashman, A. Phase behavior of flexible and semiflexible polymers in solvents of varying quality. *J. Chem. Phys.* **2019**, *151*, 034902.

(54) Sanyal, T.; Shell, M. S. Coarse-grained models using local-density potentials optimized with the relative entropy: Application to implicit solvation. *J. Chem. Phys.* **2016**, *145*, 034109.

(55) Berressem, F.; Scherer, C.; Andrienko, D.; Nikoubashman, A. Ultra-Coarse-Graining of Homopolymers in Inhomogeneous Systems. *J. Phys. Condens. Matter* **2021**, *33*, 254002.

(56) Milchev, A.; Egorov, S. A.; Midya, J.; Binder, K.; Nikoubashman, A. Entropic unmixing in nematic blends of semiflexible polymers. *ACS Macro Lett.* **2020**, *9*, 1779.

(57) Nikoubashman, A. Ordering, phase behavior, and correlations of semiflexible polymers in confinement. *J. Chem. Phys.* **2021**, *154*, 090901.

(58) Spencer, R. K. W.; Matsen, M. W. Universality of Entropic Surface Segregation from Athermal Polymer Blends Due to Conformational Asymmetry. *Macromolecules* **2022**, *55*, 1120–1126.

(59) Gō, N. Theoretical Studies of Protein Folding. *Annu. Rev. Biophys. Bioeng.* **1983**, *12*, 183–210.

(60) Poma, A. B.; Cieplak, M.; Theodorakis, P. E. Combining the MARTINI and Structure-Based Coarse-Grained Approaches for the Molecular Dynamics Studies of Conformational Transitions in Proteins. *J. Chem. Theory Comput.* **2017**, *13*, 1366–1374.

(61) Wettermann, S.; Brems, M.; Siebert, J. T.; Vu, G. T.; Stevens, T. J.; Virnau, P. A minimal Gō-model for rebuilding whole genome structures from haploid single-cell Hi-C data. *Comput. Mater. Sci.* **2020**, *173*, 109178.

(62) Lee, M. S.; Salsbury, F. R.; Brooks, C. L. Novel generalized Born methods. *J. Chem. Phys.* **2002**, *116*, 10606.

(63) Im, W.; Lee, M. S.; Brooks, C. L. Generalized born model with a simple smoothing function. *J. Comput. Chem.* **2003**, *24*, 1691–1702.

(64) Potoff, J. J.; Panagiotopoulos, A. Z. Critical point and phase behavior of the pure fluid and a Lennard-Jones mixture. *J. Chem. Phys.* **1998**, *109*, 10914.

(65) Jawerth, L. M.; Ijavi, M.; Ruer, M.; Saha, S.; Jahnel, M.; Hyman, A. A.; Jülicher, F.; Fischer-Friedrich, E. Salt-Dependent Rheology and Surface Tension of Protein Condensates Using Optical Traps. *Phys. Rev. Lett.* **2018**, *121*, 258101.

(66) Jawerth, L. M.; Ijavi, M.; Ruer, M.; Saha, S.; Jahnel, M.; Hyman, A. A.; Jülicher, F.; Fischer-Friedrich, E. Erratum: Salt-Dependent Rheology and Surface Tension of Protein Condensates Using Optical Traps [Phys. Rev. Lett. 121, 258101 (2018)]. *Phys. Rev. Lett.* **2020**, *125*, 229901.

(67) Ijavi, M.; Style, R. W.; Emmanouilidis, L.; Kumar, A.; Meier, S. M.; Torzynski, A. L.; Allain, F. H. T.; Barral, Y.; Steinmetz, M. O.; Dufresne, E. R. Surface tensiometry of phase separated protein and polymer droplets by the sessile drop method. *Soft Matter* **2021**, *17*, 1655–1662.

(68) Goebel, A.; Lunkenheimer, K. Interfacial Tension of the Water/n-Alkane Interface. *Langmuir* **1997**, *13*, 369–372.

(69) Zeppieri, S.; Rodríguez, J.; López de Ramos, A. L. Interfacial Tension of Alkane + Water Systems. *J. Chem. Eng. Data* **2001**, *46*, 1086–1088.

(70) Widom, B. Surface tension and molecular correlations near the critical point. *J. Chem. Phys.* **1965**, *43*, 3892.

Graphical TOC Entry